Effects of temperature on autogenous deformation and early-age stress evolution in cement pastes with low water to cement ratio

Liang, Minfei; Liu, Chen; Liang, Xuhui; Chang, Ze; Schlangen, Erik; Šavija, Branko

DOI
10.1016/j.conbuildmat.2023.134752

Publication date
2023

Document Version
Final published version

Published in
Construction and Building Materials

Construction and Building Materials 411 (2024) 134752

Contents lists available at ScienceDirect

Construction and Building Materials

journal homepage: www.elsevier.com/locate/conbuildmat

Effects of temperature on autogenous deformation and early-age stress evolution in cement pastes with low water to cement ratio

Minfei Liang [a,1,*], Chen Liu [a,1], Xuhui Liang [a], Ze Chang [b], Erik Schlangen [a], Branko Šavija [a]

[a] Microlab, Faculty of Civil Engineering and Geosciences, Delft University of Technology, Delft 2628 CN, the Netherlands
[b] Department of Mechanical Engineering, Eindhoven University of Technology, Eindhoven 5600 MB, the Netherlands

ARTICLE INFO

Keywords:
Autogenous deformation
Early-age cracking
Creep/ relaxation
Stress evolution
Temperature

ABSTRACT

This paper investigates the influence of temperature on autogenous deformation and early-age stress (EAS) evolution in ordinary Portland cement paste using a recently developed Mini Temperature Stress Testing Machine (Mini-TSTM) and Mini Autogenous Deformation Testing Machine (Mini-ADTM). In the Mini-TSTM/ ADTM, CEM I 42.5 N paste with a water-cement ratio of 0.30 was tested under a curing temperature of 10, 15, 20, 25, 30, and 40 °C. X-Ray diffraction (XRD) tests were conducted to measure the amount of ettringite and calcium hydroxide, which reveals the micro-scale mechanisms of autogenous expansion. The applicability of the Maturity Concept (MC) for the prediction of autogenous deformation and relaxation modulus under different temperatures was also examined by the experimental data and the viscoelastic model. This paper leads to the following findings: 1) The autogenous deformation of ordinary Portland cement paste is a four-stage process comprising the initial shrinkage, autogenous expansion, plateau, and autogenous shrinkage; 2) Higher temperature leads to higher early-age cracking (EAC) risk because it accelerates the transitions through the first three stages and causes the autogenous shrinkage stage to start earlier. Moreover, higher temperatures also result in increased rates of autogenous shrinkage and EAS in the autogenous shrinkage stage; 3) Autogenous expansion and plateau are attributed to the crystallization pressure induced by CH. Temperature-dependent CH formation rates determine the duration of the plateau stage; 4) Low-temperature curing can delay but not completely prevent the EAC induced by autogenous deformation; 5) The MC cannot predict the autogenous deformation at different temperatures but can be used to calculate the relaxation modulus, which in turn aids in EAS prediction based on autogenous deformation data.

1. Introduction

Early-age cracking (EAC) is a common issue in construction of concrete structures. When the volumetric deformation is restrained, early-age stress (EAS) builds up in the concrete, potentially resulting in EAC if the EAS exceeds the tensile strength. There are mainly three kinds of deformation that can induce the EAS buildup: thermal, drying, and autogenous deformation (AD) [1,2]. The thermal and drying deformation are related to the transfer of heat and moisture between the structures and the environment, and therefore they not only depend on the material itself but also the environment and structural design [3,4]. The use of supplementary cementitious materials (SCMs) (to reduce the total hydration heat) [2,5] and proper curing measures (to prevent moisture loss) [6] have been reported to effectively decrease the risk of EAC related to thermal and drying deformation. On the other hand, the main process of AD, mostly known as the "self-desiccation shrinkage", arises from the consumption of pore water by the hydration reaction and directly relates to the hydration of the cementitious material [7]. Note that such self-desiccation shrinkage is an important factor inducing EAC, but it is only one component of AD, which will be explained in detail in the main part of this paper. High-performance concrete (HPC) and ultra-high-performance concrete (UHPC) have a significantly higher risk of AD-induced EAC due to low water/ binder ratios [8–10]. Therefore, the EAC risk induced by AD in low water/ binder ratio deserves in-depth investigation.

The mechanism of AD ε_{ad} is shown in Fig. 1. During the formation of

* Corresponding author.
E-mail addresses: M.Liang-1@tudelft.nl (M. Liang), C.Liu-12@tudelft.nl (C. Liu), X.Liang-1@tudelft.nl (X. Liang), Z.chang@tue.nl (Z. Chang), Erik.Schlangen@tudelft.nl (E. Schlangen), B.Savija@tudelft.nl (B. Šavija).
[1] These authors contributed equally to this work.

https://doi.org/10.1016/j.conbuildmat.2023.134752
Received 2 October 2023; Received in revised form 20 December 2023; Accepted 22 December 2023
Available online 28 December 2023

the solid microstructure, the chemical shrinkage (defined as the absolute volume reduction of the material [11]) leads to formation of capillary pores, which afterwards enables the self-desiccation process under the effects of continuous hydration reaction, contributing to a major part of AD. In general, AD mainly comprises two parts: the autogenous expansion ε_{ep} and autogenous shrinkage ε_{sd}. By definition, AD should be tested on a sealed specimen under constant temperature. A strictly-constant temperature over the whole specimen is difficult to achieve, which requires not only constant room temperature but also active heating/ cooling procedure to compensate for the hydration heat release. Therefore, it is quite common that temperature variations exist in most tests and thus thermal deformation ε_{th} will also be included in the measurement as the apparent autogenous deformation, influencing the testing accuracy of the true AD ε_{ad} [12]. Comparing to the expansion, the autogenous shrinkage ε_{sd} is the direct reason for the EAC risk. Continuous hydration consumes pore water (i.e., self-desiccation), resulting in the RH drop and capillary pressure buildup, which further leads to contraction of the microstructure and therefore shrinkage [13]. Another part of AD, the autogenous expansion ε_{ep}, happens mainly because the expansive products such as calcium hydroxide (CH) or ettringite apply crystallization pressure on the pore walls and causes the expansion [14–18]. However, such autogenous expansion is often neglected or underestimated [19], potentially because of a late starting time of AD tests which may overlook the expansion phase [16], lack of temperature control causing influence of thermal deformation [12], or different cement compositions.

AD tests have mostly been conducted on sealed specimens under constant temperature to exclude the influence of drying/ thermal deformation and different hydration kinetics [20–22]. However, the results of such tests can only provide limited guidance on real-world applications with varying temperatures. According to Klausen et al. [23], AD tested under a realistic temperature history differed significantly from that under constant temperature. In the field of cementitious materials, the maturity concept (MC) [24] has been widely used to convert the mechanical properties of specimens cured under a constant temperature to that of specimens exposed to a realistic temperature history. The assumption for the MC is that temperature only influences the hydration rate, and that this influence is independent of the hydration degree. However, except for the hydration rate, the temperature also leads to changes in RH and surface tension, which questions the applicability of the MC in AD prediction [25–27].

The exact influence of temperature on AD is complex because temperature not only influences the RH drop and surface tension but also results in different pore structures [28], which are all related to the self-desiccation effects [13]. Lura et al. [29] performed AD tests from 10 to 40 °C and found that higher temperatures lead to earlier onset of shrinkage but not necessarily to higher deformations. Similarly, Carette et al. [15] suggested an earlier onset of shrinkage when the temperature is higher. Furthermore, they also concluded that, due to the higher RH, coarser porosity, increased solubility and decreased needle size of ettringite, the higher temperature tends to decrease the total amplitude of both autogenous expansion and self-desiccation shrinkage. However, Orosz et al. [12] observed an opposite trend, i.e., that higher temperature leads to higher autogenous expansion, but they also mentioned that the lack of data on coefficient of thermal deformation may compromised their measurement. Contradictory findings regarding the influence of temperature on autogenous shrinkage were also found: with increasing temperature, the studies [15,30,31] observed decreased autogenous shrinkage while others [27,32,33] saw an increased one. Maruyama et al. [34] conducted AD tests on UHPC and found that the influence of temperature was different before and after a so-called inflection point. The "inflection point" was defined as a specific stage in the development of AD, characterized by a significant change in shrinkage behavior, typically occurring between 10 and 16 h of equivalent age. Before the inflection point, the AD decreased with increasing temperature and then increases afterward.

In summary, the exact influence of temperature on AD is debatable and the applicability of MC in predicting AD at different temperatures is questionable. Moreover, most studies only focused on AD but neglected the measurement of EAS, which is a combined result of AD and viscoelastic properties and is a more straightforward indicator of EAC risk [35]. There are many tests allowing the measurement of EAS, including the ring test, plate test, longitudinal test, and substrate restraint test [36, 37]. Among these tests, the Temperature Stress Testing Machine (TSTM) stands out with advantages in explicit and flexible mechanical loading schemes, active temperature control, and tunable restraint degree [38]. However, the TSTM demands complex testing facilities and substantial workforces [39], which hinders the EAS test over many parameters.

In this paper, autogenous deformation and EAS of ordinary Portland cement paste will be tested under different curing temperatures, based on the Mini-TSTM and Mini-ADTM developed in [40]. Detailed analysis of the influence of curing temperatures on autogenous deformation will be conducted based on the results of AD, EAS, and hydration products (tested by X-Ray diffraction (XRD)). Furthermore, based on a viscoelastic model, the applicability of MC for prediction of AD, EAS, and relaxation modulus in EAC analysis will be examined. This paper aims to

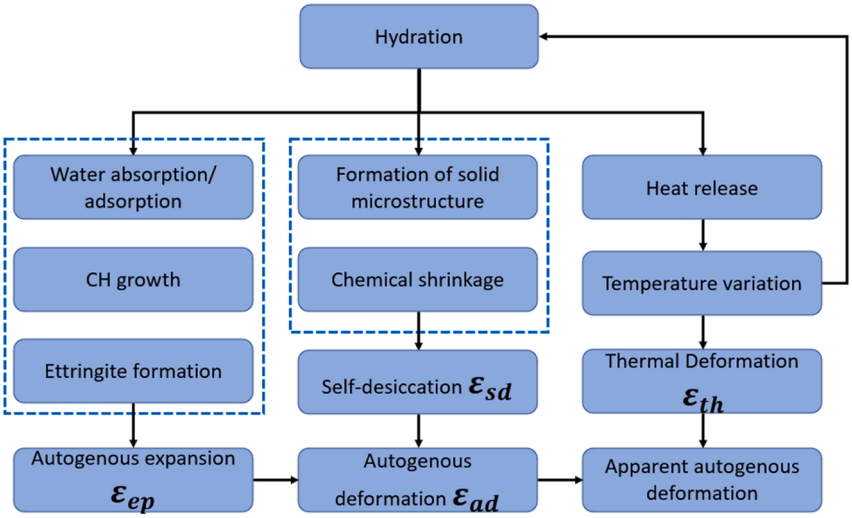

Fig. 1. Mechanisms of autogenous deformation of cementitious materials (adapted from [15]).

provide an in-depth understanding of the influence of temperature on autogenous deformation and guidance for preventing early-age cracking induced by autogenous deformation.

2. Methods

2.1. Materials

The EAS and AD of CEM I 42.5 paste with a w/c ratio of 0.30 were tested by Mini-TSTM and Mini-ADTM respectively. The chemical compositions of the cement are shown in Table 1. The AD and corresponding EAS evolution of cement paste under six different temperatures (i.e., 10 °C, 15 °C, 20 °C, 25 °C, 30 °C, 40 °C) were tested. The tests for the temperatures 10 °C and 15 °C started 6 h after the casting, while for 20 °C, 25 °C, 30 °C and 40 °C, the tests started 4 h after casting. The temperature control is guaranteed by a cryostat, which pumps heating/ cooling water to circulate in the Mini-TSTM/ ADTM. To show the effectiveness of temperature control, the heating/ cooling process of the test at 40 °C is shown in Fig. 2. After casting, the temperature of the specimen is around 25 °C, and the water pumped out from the cryostat is around 31 °C. In order to heat the specimen to 40 °C, the cryostat heated the water to over 53 °C and then decreases to around 40 °C to keep the temperature in the specimen stable. The heating process of the specimen from 25 °C to 40 °C takes about 10 min, which is considered negligible to the measurement of autogenous deformation and stress measured at a more hardened state. The tests lasted until the specimens cracked, which happened for all the specimens in this study before 168 h. For each test, two specimens can be casted for the Mini-ADTM and Mini-TSTM test, which will be introduced in detail in the Section 2.2.

2.2. Mini-TSTM/ ADTM tests

The general principle of a typical TSTM system is shown in Fig. 2. The TSTM system is composed of two parts, a restraint test with a dog-bone specimen and a free test with a specimen of a similar geometrical size as the dog-bone one. Liner Variable Differential Transducers (LVDTs) are used in both specimens to measure the deformation in the center part. In the dog-bone specimen, the measurement of LVDT controls the load F based on a feedback loop FL1 to achieve the full restraint condition. Cryostat is used for circulating water around the specimen to maintain a constant temperature based on the temperature measurement T_c in the specimen and a feedback loop FL2.

Following such principles, a Mini-TSTM system has been recently developed [40], which focuses on improvement in testing efficiency, as shown in Fig. 3. The design of the Mini-ADTM system is similar to the TSTM system and therefore is not shown here. The mold is shown in the middle of Fig. 3(a), consisting of three covering plates (C1, C2, C3), two side plates (S1, S2), two crosshead plates (CH1, CH2), and a back plate (B1). The strain of the specimen is measured by two inductive LVDTs at the two sides of the mold, as shown in the left of Fig. 3(a). The measurement range of the adopted LVDT is ± 1 mm, and the precision is 0.01 μm. The LVDTs are connected with invar bars and attached to two steel bars embedded in the specimen using magnetic blocks. The red plugs are used to hold the bars before the specimen is hardened enough

Table 1
Oxide compositions of the adopted cementitious materials (% wt.).

Composition	CEM I
CaO	64.00
SiO_2	20.00
Al_2O_3	5.00
MgO	-
SO_3	2.93
Fe_2O_3	3.00
Na_2O	0.58

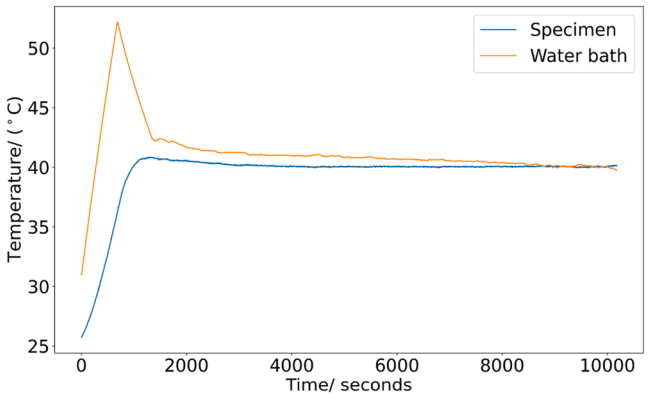

Fig. 2. Temperature measurement before starting the TSTM test at 40 °C.

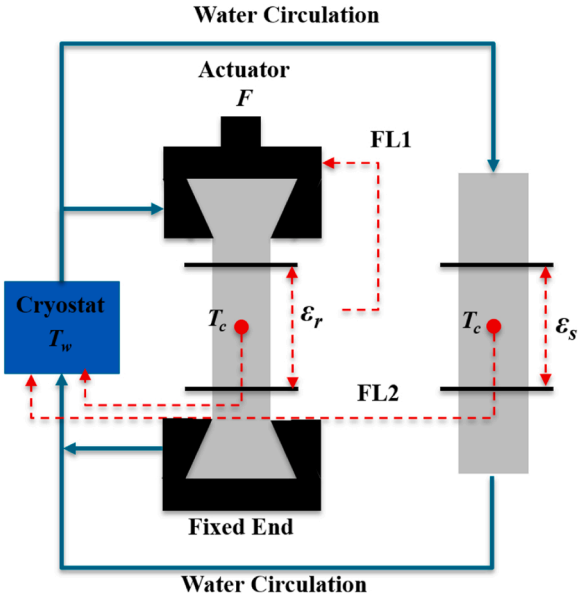

Fig. 3. Schematic diagram of a TSTM system [40].

to start the tests. Given the strain measurement as the input, a proportional-integral-derivative (PID) controller is used to continuously adjust the load of a universal loading machine (Fig. 3(b)) to keep the strain in the specimen (between the embedded steel bars over a measuring length of 100 mm) at 0, so as to achieve the full-restraint condition. The temperature control of this test is achieved by circulating water through each plate (right part of Fig. 3(a) and Fig. 3(d)). The water temperature is controlled by a cryostat using a PID controller, based on the input of temperature measured by a thermocouple embedded in the center of the specimen. After casting the fresh material in the mold, the AD, EAS, and viscoelastic properties can be tested under free condition, full-restraint condition, and load-controlled condition with an hourly-repeated loading scheme [40–42], respectively.

2.3. X-Ray diffraction (XRD) test

The XRD test aims to investigate the influence of temperature on the amount of expansive hydration products CH and ettringite at three different ages. The specimens cured under 20 °C and 40 °C will be used. First, the specimens are broken into small pieces and immersed in isopropanol to stop hydration. Then, the specimens are ground into powder for 20 min. Finally, the powder is filtered out and placed in an oven of 40 °C for 5 min. The XRD test was carried out on a Philips PW 1830/40 powder diffractometer using the Cu K-alpha radiation. The adopted

acceleration voltage was 40 kV and the X-ray beam current was 40 mA. The XRD data were collected with a step size of 0.03° for a 2θ range from 5° to 60°. The exact ages of the specimens for the XRD tests depend on the specific AD pattern and will be discussed in Section 3.3.

2.4. Maturity concept (MC)

The MC assumes that the influence of temperature on the hydration rate is independent of the hydration degree, and can be described by the following equation [24]:

$$\frac{d\alpha}{dt} = g(\alpha)f(T) \tag{1}$$

where α is the hydration degree; functions $g(\alpha)$ and $f(T)$ quantify the effects of hydration degree and temperature on the hydration rate, respectively. The function $f(T)$ is the so-called time-temperature function (TTF). The degree of hydration can then be quantified by integrating Eq.(1) as follows:

$$\int_0^{\alpha} \frac{d\alpha}{g(\alpha)} = \int_0^{t} f(T(\tau))d\tau \tag{2}$$

Eq.(2) further leads to the definition of maturity function $M(t)$ as the integration of TTF over time, normalized by a constant obtained at a reference temperature:

$$M(t) = \int_0^{t} \frac{f(T(\tau))}{f(T_{ref})}d\tau \tag{3}$$

Based on different TTF, Eq.(3) gives different expressions of maturity index. Using the Arrhenius equation, the expression of the so-called equivalent age can be derived [24]:

$$M(t) = \int_0^{t} \exp\left(\frac{E_a}{R}\left(\frac{1}{273+T_{ref}} - \frac{1}{273+T(\tau)}\right)\right)d\tau \tag{4}$$

where E_a is the activation energy of ordinary Portland cement; R is the universal gas constant (i.e., 8.314 J/ (K· mol)); T_{ref} is the reference temperature, which is 20 ℃ in this paper. The value for apparent activation energy E_a is dependent on the cement type and temperature. The activation energy increases when the temperature is lower than 20 ℃ but remains constant when temperature is equal to or higher than 20 ℃ [43]. Based on tests, the following bilinear relationship for apparent activation energy has been proposed [24]:

$$E_a = \begin{cases} E_{a0}, if \quad T \geq 20℃ \\ E_{a0} + 1470(20-T), if \quad T < 20℃ \end{cases} \tag{5}$$

where E_{a0} is the apparent activation energy of a certain cement type at 20 ℃. In this study, the value of 40500 J/mol for the activation energy E_{a0} of ordinary Portland cement tested as tested in [44] is used.

2.5. Viscoelastic model

The EAS evolution can be calculated by a viscoelastic model, as in [4,45–47]. The Mini-TSTM test focuses on the straight part of the dog-bone specimen, where the stress should be evenly distributed. Therefore, the Mini-TSTM test can be seen as a 1-D uniaxial loading scenario. The EAS evolution in the Mini-TSTM is a relaxation process, described by the principle of Boltzmann superposition as below:

$$\sigma(t) = \int_0^{t} R(t_0, t)\dot{\varepsilon}(t_0)dt_0 \tag{6}$$

where σ is the EAS; ε is the imposed strain; R is the relaxation modulus; t_0 is the time when the deformation is imposed; t is the current time. By using the mid-point rule, the Eq. (4) can be simplified as:

$$\sigma(t) = \sum_{t_0=0}^{t_0=t} R(t_0, t+\frac{1}{2}\Delta t) \times \Delta\varepsilon(t_0) \times \Delta t_0 \tag{7}$$

The relaxation modulus can be derived from the creep compliance, which is easier to test. The creep compliance can be described by the double power law [48,49] as below:

$$J(t_0, t) = \frac{1}{E(t_0)} + a * \left(\frac{1}{t_0}\right)^{b} * (t-t_0)^{c} \tag{8}$$

where a, b and c are fitting parameters that can be derived from tests, which for CEM I 42.5 paste with a water/ cement ratio of 0.30 at 20 ℃ are 1.0×10^5, 1.079, and 0.5, respectively, according to the load-controlled Mini-TSTM test in [40]. Then, the relaxation modulus can be derived as follows [50–52]:

$$R(t, t_0) = e^{1-J(t_0,t)E(t)}E(t) \tag{9}$$

Afterward, the creep and elastic modulus under different temperatures can be calculated by the MC as Eq((4)-(5)). Finally, using the AD measured under different temperatures, and the relaxation modulus under different temperatures calculated using Eq ((8)-(9)) and the MC, the EAS under different temperatures can be calculated using Eq. (7). To evaluate the accuracy of the prediction, the root mean square error is calculated, as below:

$$RMSE = \sqrt{\frac{\sum_t(\sigma_M(t) - \sigma_T(t))^2}{t_{total}}} \tag{10}$$

where $\sigma_M(t)$ and $\sigma_T(t)$ are modelling and testing results of EAS at time step t.

3. Results and discussion

3.1. Autogenous deformation

The results of EAS and AD of cement paste under six different temperatures are shown in Fig. 4. The stress results (Fig. 4(a)) show clearly that the EAS evolution all begins with compression, goes into tension, and then cracks when the EAS exceeds the tensile strength. When the temperature increases, the EAC happens much faster: under 10 °C, the EAC happens at around 140 h, while the EAC timing under 40 °C is around 11 h. However, an exception is the result at 25 °C, in which the strength development seems to be fast and therefore the timing of EAC is later than that of 20 °C. Another reason for such delayed cracking may be the scatter of the test. On the other hand, it is also worth noting that for lower temperatures, a plateau can often be found at the transition from compression to tension, which seems to delay the EAC.

The results of AD (Fig. 4(b)) indicate that the AD mostly begins with initial shrinkage, then expansion, and finally shrinkage. An exception is the result at 40 °C, where only the expansion and shrinkage are observed because the starting time of the test at 40 °C is 4 h, when the initial shrinkage has probably already finished, and the expansion has begun. As suggested by Yoo et al [53], the time-zero for measurement of AD should be the onset of the EAS development, which makes sense because the EAS is a more direct index to evaluate the EAC risk. In this study, it was found that the EAS before the onset of expansion measured at all temperatures are trivial (i.e., below 0.02 MPa), due to the low elastic modulus and high creep [18,54]. Moreover, the measurement of the exact magnitude of initial deformation is scattered [55–57]. Therefore, to exclude the influence of initial shrinkage, the time-zero of AD is set at the onset of expansion, which is around 15, 12, 10, 8, 7 and 5 h after casting for the temperatures of 10 °C, 15 °C, 20 °C, 25 °C, 30 °C, and 40 °C respectively, as shown in Fig. 4(c). The results clearly show the influence of temperature on AD: higher temperatures result in faster expansion within shorter duration. Besides, higher temperatures also

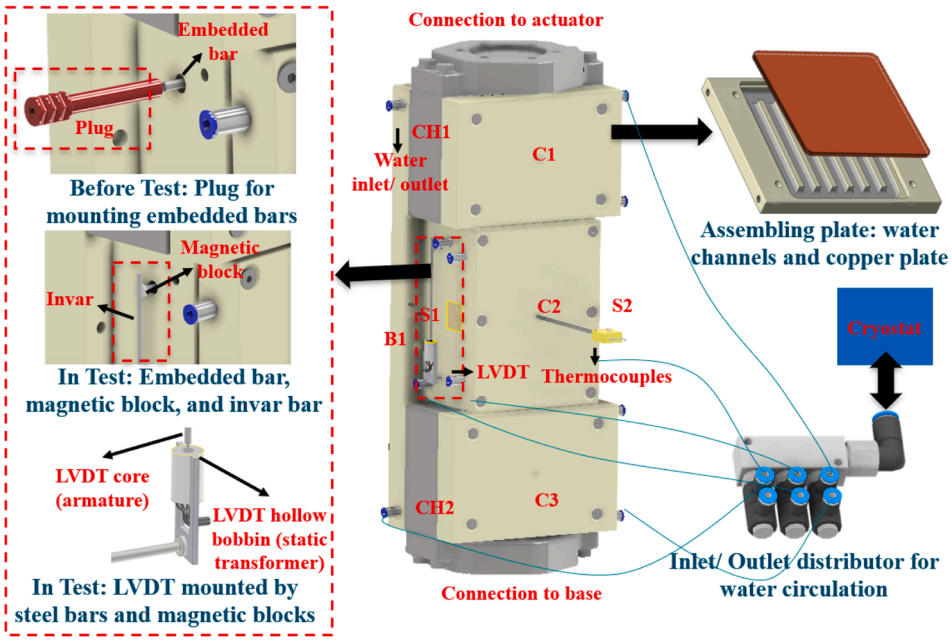

(a)

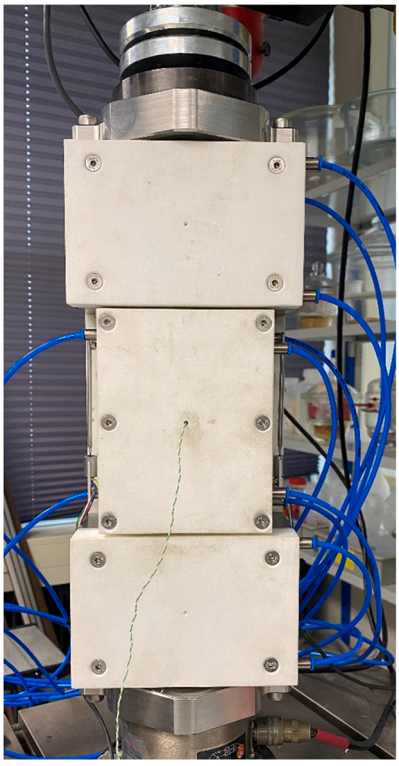

(b)

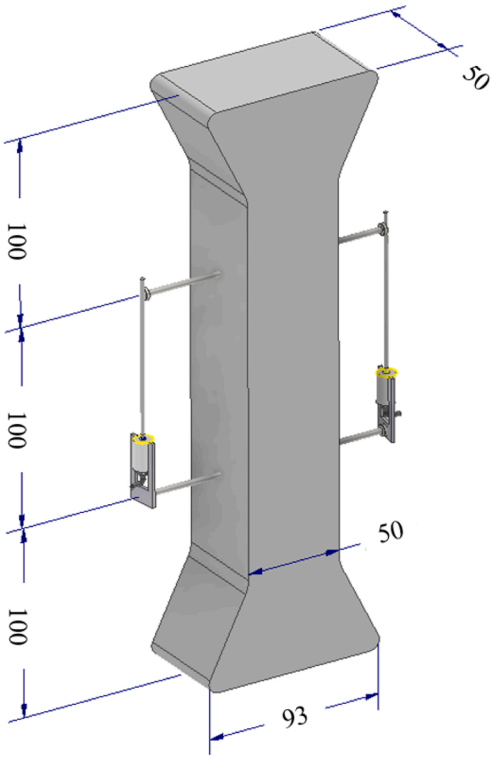

(c)

Fig. 4. The mini-TSTM: (a) overall design; (b) the efficient TSTM installed in the loading machine; (c) geometry of the dog-bone specimen (unit: mm); (d) parallel connection of water circulation system. [40].

induce faster transition from expansion to shrinkage. A much longer plateau can be found for a lower temperature at the transition from expansion to shrinkage. At 30 °C, the plateau seems to be gone, but a noticeable slowing down in the development of shrinkage and stress at the transition of expansion and shrinkage can still be observed. Such plateau completely disappears when the temperature reaches 40 °C.

The results in Fig. 4 show that, in accordance with the MC, the increased temperature accelerates the development of AD and EAS. This is especially clear if one looks at the EAS results (Fig. 4(a)): the EAS at lower temperatures seems to be a stretched version along the time axis of

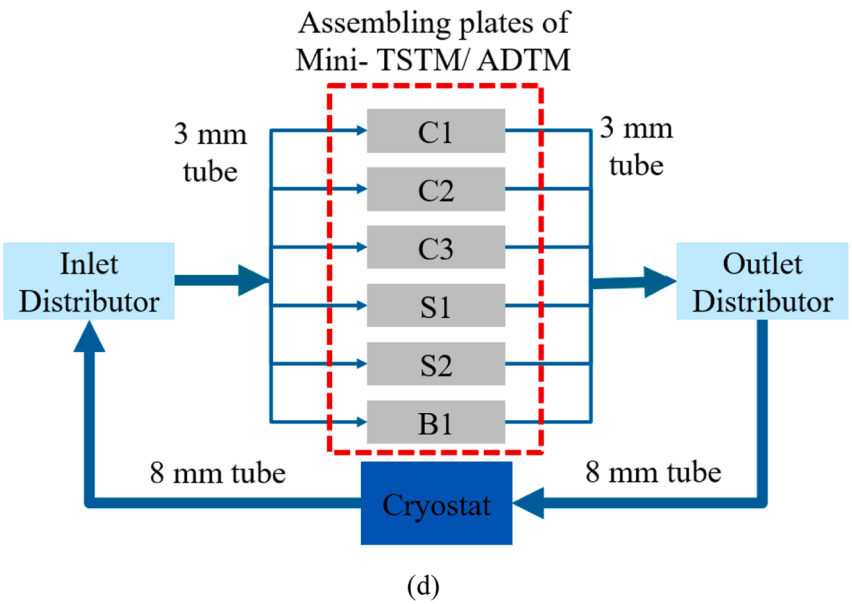

Fig. 4. (*continued*).

that at higher temperatures. On the other hand, the AD (Fig. 4(b, c)) does not show such effect clearly because the scatter in measurement of initial shrinkage and expansion may not convey meaningful indication about the influence of temperature on the magnitude of AD.

However, the existence of a plateau at the expansion-shrinkage transition significantly changes the shape of the curves, which indicates that a strict time-scaling effect like that of the MC may not be valid. This can be directly examined by applying the Eq((4)-(5)) to calculate the equivalent ages under the six different temperatures and replot the results in Fig. 4 with respect to the calculated equivalent ages as shown in Fig. 5. If a strict time-scaling effect such as MC stands, the AD and EAS with respect to the equivalent age under different temperatures should show the same pattern. To some extent, Fig. 5 shows that the MC can predict the peak of compressive stress (Fig. 5(a)) and expansion (Fig. 5(b)) in a seemingly consistent way. However, Fig. 5 also shows that different plateaus are obtained under different temperatures. In 30 °C and 40 °C, the plateaus almost disappear. Moreover, after the plateau, the shrinkage rate is also different: the shrinkage rates evaluated by the equivalent age in 30 °C and 40 °C are slower than those below 30 °C, indicating that the MC can overestimate the AD development if a prediction for AD at a higher temperature is made based on the AD at a low or medium temperature. Such overestimation is because MC only considers the accelerated hydration reaction under high temperatures, which can accelerate water consumption and therefore promote the self-desiccation shrinkage [13]. Meanwhile, MC neglects other factors, such as the fact that higher temperatures tend to cause higher porosity [28], which can decrease the capillary pressure induced by self-desiccation, and therefore limit the acceleration of AD development. Therefore, the MC does not fully quantify the changes of AD under different temperatures.

3.2. Four-stage process

In general, the AD and EAS demonstrate four stages, as shown in Fig. 6. The consistency between the EAS and AD in Fig. 6, that the compressive/ tensile stress corresponds to the autogenous expansion/ shrinkage, also validates the reasonability of the Mini-TSTM/ ADTM tests. More importantly, the process of the four stages is given as below:

1) Stage 1 (S1): the initial deformation before the onset of autogenous expansion and compressive stress, which is mostly induced by chemical shrinkage and settling of the fresh material after casting [56]. In S1, the material is still very soft and has very low elastic modulus and high creep, so the stress is very low and can almost be neglected. Therefore, although the magnitude of the deformation in this stage is very scattered among different batches of tests for the same type of cement paste, as also observed by other studies [55], its influence can be neglected. Note that, although various studies have given indirect definitions for time-zero such as the rate of relative humidity and setting time [58–60], the onset of EAS evolution is the most straightforward definition of time-zero because the EAS is the direct index for EAC risk assessment. Therefore, the end of the S1 is exactly the time-zero after which the AD should be considered in stress calculation.
2) Stage 2 (S2): the autogenous expansion, which is induced by crystal growth such as formation of ettringite [17,18,61,62] and calcium hydroxide (CH) [63]). Note that the Mini-TSTM/ ADTM tests are all conducted under constant temperatures, so the significant autogenous expansion in S2 is not a result of thermal deformation. In S2, an apparent expansion happens and induces compressive stress in the restrained specimens. The magnitude of these compressive stress is low, but it counteracts the tensile stress happening later. To quantify this compressive stress, accurate data of the viscoelastic properties is essential because creep at this stage is very high.
3) Stage 3 (S3): the transition from autogenous expansion to self-desiccation shrinkage, which shows as a plateau of AD and EAS at low and medium temperatures (Fig. 6(a-d)), indicating a slow transition process. When temperature is higher, such plateau disappears, and the autogenous shrinkage occurs much sooner. A slow transition from autogenous expansion to autogenous shrinkage can delay the occurrence of tensile stress and therefore lower the EAC risk.
4) Stage 4 (S4): the self-desiccation shrinkage, which induces fast development of tensile stress and directly causes EAC [64]. In this stage, despite the rate of shrinkage is not necessarily higher than some deformation in S1 and S2, but due to the higher elastic modulus and lower creep/ relaxation, the EAS accumulates much faster and poses higher EAC risk.

Overall, in S1∼S3, the magnitude of EAS is limited because of very low elastic modulus and high creep in S1 and S2 and slow deformation rate in S3. In fact, S4 is the stage that really induces the EAC risk. Therefore, regarding the influence of AD on EAS evolution and EAC risk,

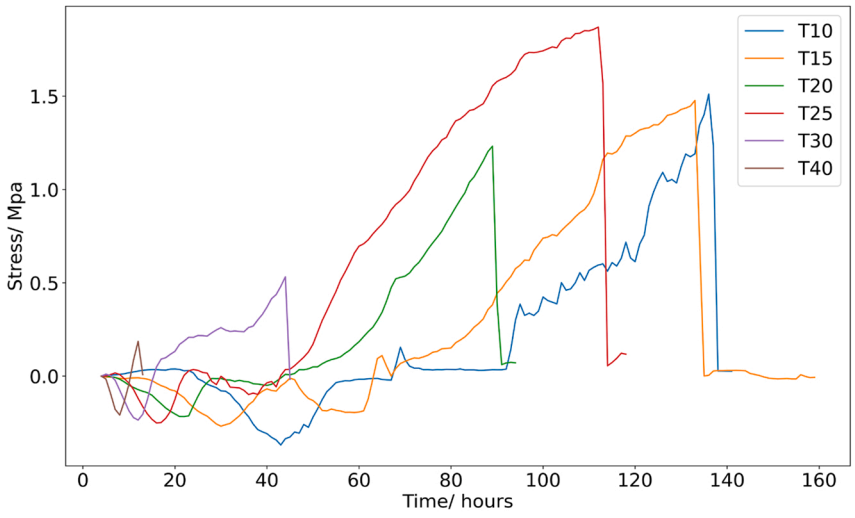

(a)

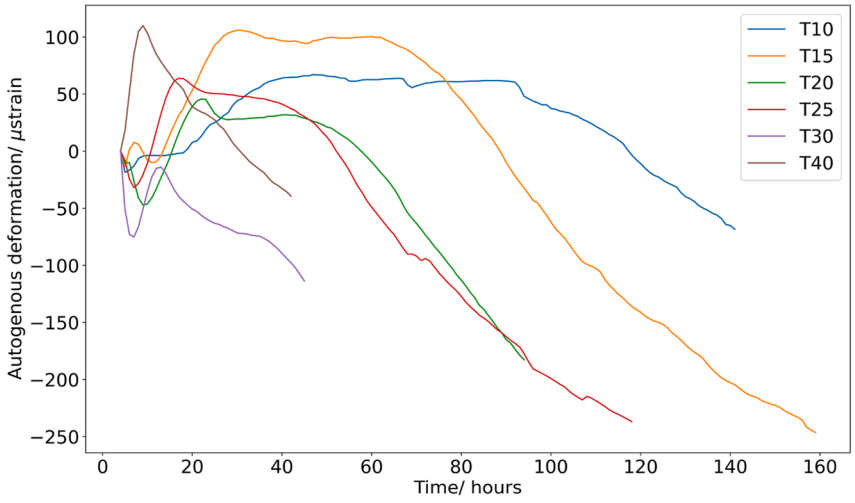

(b)

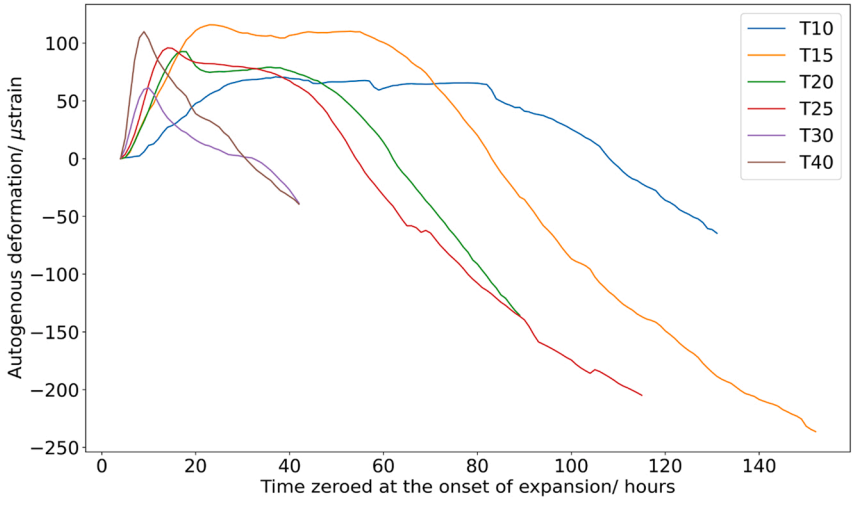

(c)

Fig. 5. The AD and EAS of cement paste under 6 different temperatures: (a) EAS; (b) AD; (c) AD with the time-zero being the onset of autogenous expansion.

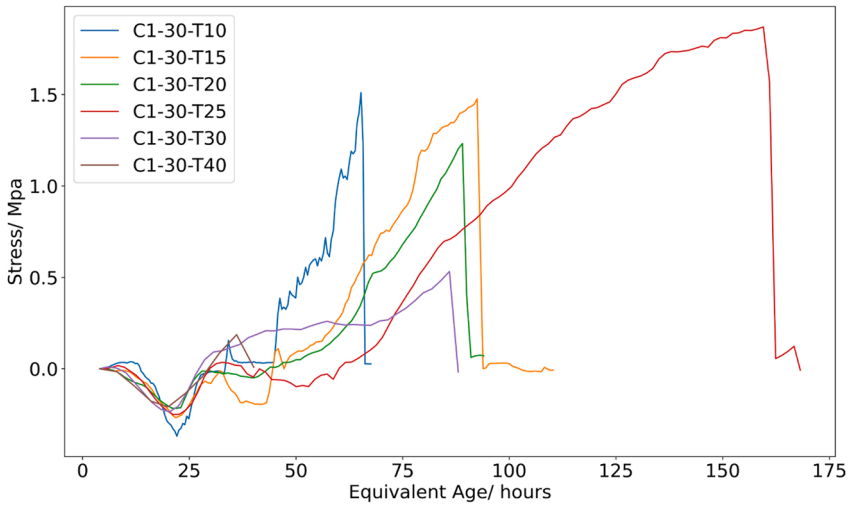

(a)

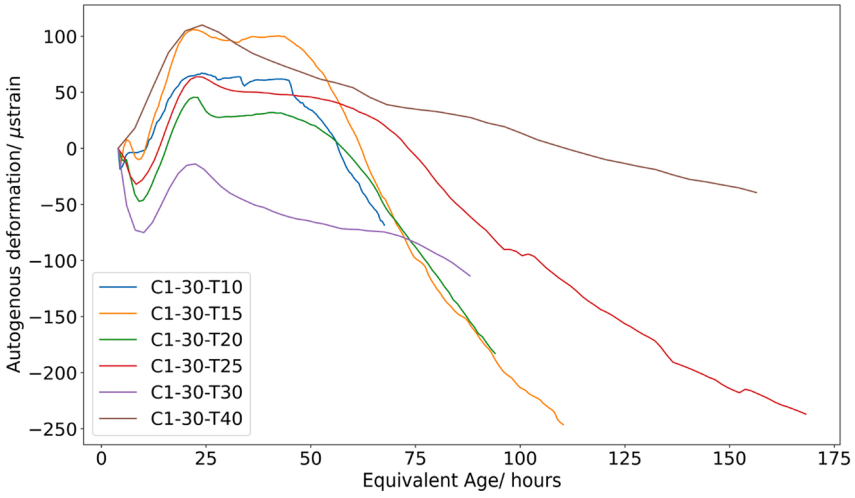

(b)

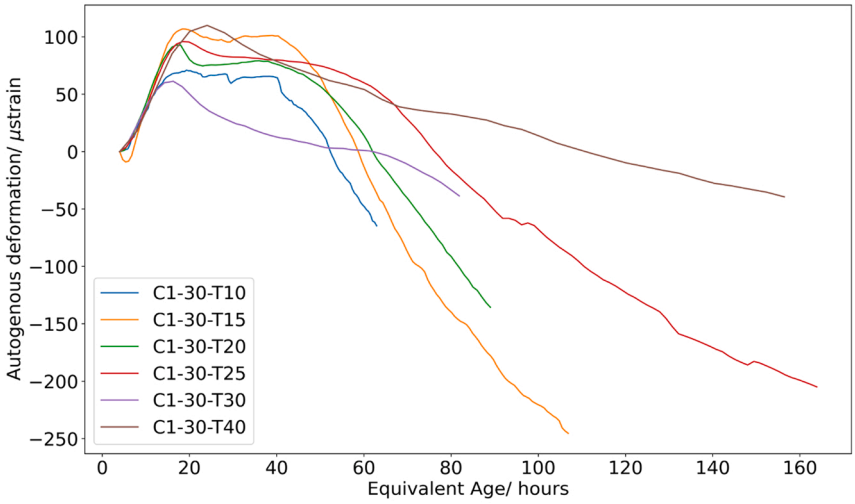

(c)

Fig. 6. The AD and EAS of cement paste with respect to the equivalent age calculated by the MC: (a) EAS; (b) AD; (c) AD with the time-zero being the onset of autogenous expansion.

the duration of the S1~S3 matter much more than the magnitude of the AD happening in corresponding period, because the duration of the three stages determines when the S4 will begin. Fig. 7 clearly shows the influence of the temperature on the duration of each stage:

1) As temperature increases, the duration of S1 is shortened, which is similar to the decrease of setting time in higher temperatures as observed in [63,65,66].
2) As temperature increases, the S2 begins earlier, and its duration is shorter.
3) The duration of S3 follows a decreasing trend as the temperature increases. In 30 °C, the plateau is not apparent, but the shrinkage and tensile EAS increases gradually from a lower rate (Fig. 6(e)). In 40 °C, the S3 disappears, indicating a direct transition from autogenous expansion (S2) to autogenous shrinkage (S4) and therefore higher EAC risk.
4) The end of the S4 is the timing of EAC. The results show that, as temperature increases, the EAC happens earlier, except for the results in 25 °C. Reasons for such inconsistency may be the faster and more thorough strength development under 25 °C or the scatter of the Mini- ADTM/ TSTM tests.

In summary, this section describes the four-stage process. In S1, there is no stress in the specimen (i.e., time-zero) and therefore the analysis can start from the S2. Two essential aspects that influence the EAC risk are: 1) the duration of S2~S3 which determine the onset of S4 and 2) the rate of autogenous shrinkage and EAS evolution in S4. These two aspects will be investigated in detail in the following sections.

3.3. Autogenous expansion in S2~S3 due to CH formation

The autogenous expansion in S2 is induced by crystal formation of either ettringite [61,62] or calcium hydroxide [63], which can both be detected and quantified by XRD tests. To investigate the influence of temperature on the AD and EAS in S2~S3, samples cured at 20 and 40 °C are selected for the XRD tests, at three specific ages: 1) the age at

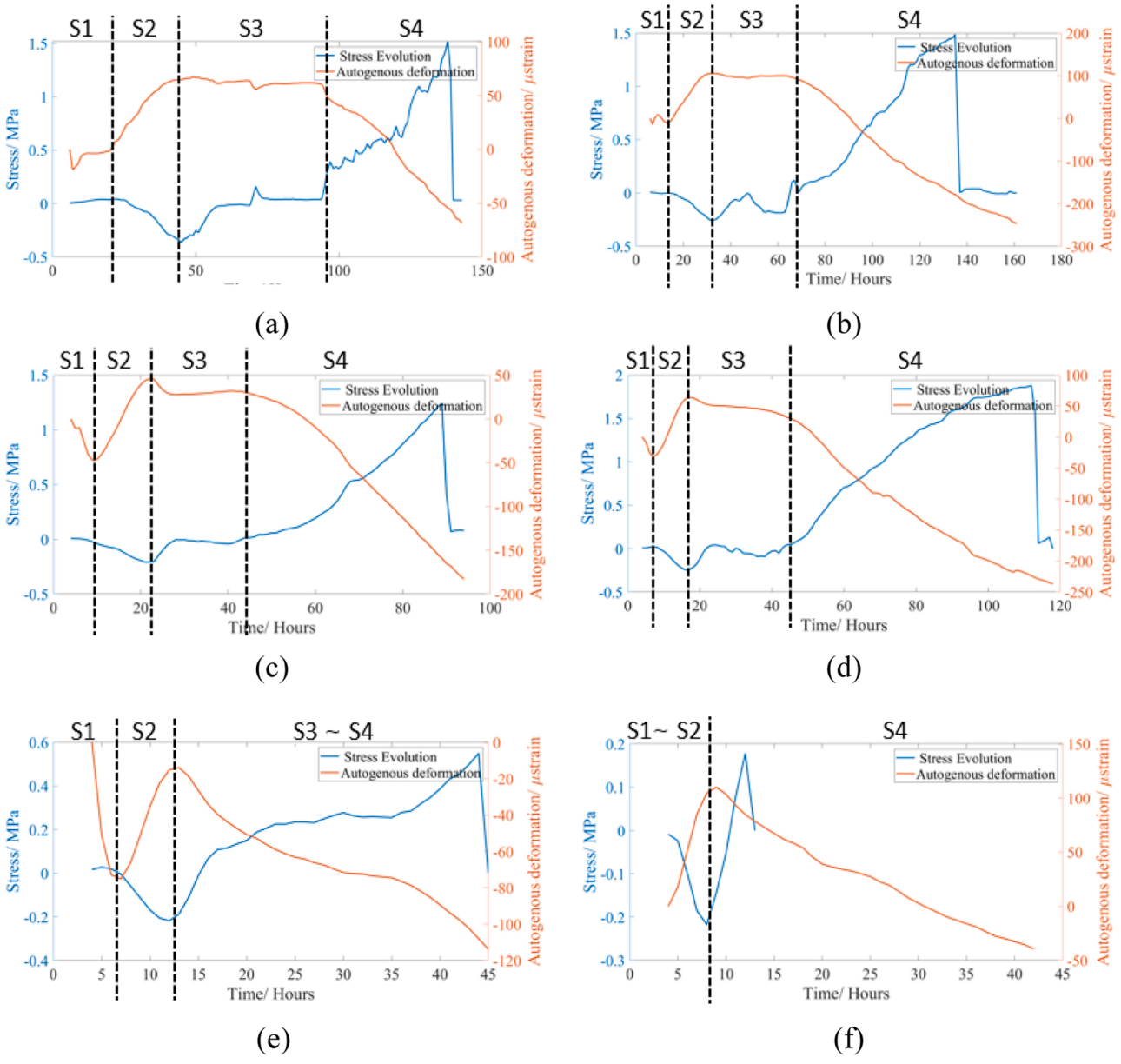

Fig. 7. The four-stage process of the AD and EAS evolution under six different temperatures: (a~ f) corresponds to the temperatures of 10 °C, 15 °C, 20 °C, 25 °C, 30 °C, and 40 °C respectively (Note that the scales of x-axis are different).

the onset of expansion (i.e., beginning of the S2); 2) the age at the end of expansion (i.e., end of the S2); and 3) an age in S4. As a result, the selected ages are 9 h, 23 h, and 54 h for the samples cured at 20 °C and 4 h, 9 h and 24 h for the samples cured at 40 °C. The curing temperatures are ensured by a cryostat. Before the XRD test, 10 wt% silicon was added to the sample powder as an internal standard, and then Rietveld refinement [67] was conducted to decompose the raw XRD curve. Note that Rietveld refinement is necessary if quantification of the percentages of the crystal are needed. Due to the variations in sample preparations and testing conditions, the total intensity in each measurement varies from each other. And therefore, the peak intensity between different tests cannot be directly used to compare the percentage of a certain mineral. Using Rietveld refinement, which normalizing the measured intensities with the intensity of the controlled internal standard, such variations between different testing batches can be avoided and therefore can produce reliable quantification results. By predefining the mineral types of different hydration products and clinkers, the decomposition is conducted based on the program BGMN [68] and the ICDD database. As shown in Fig. 8, a good fit was obtained for XRD patterns of all samples, whose weighted profile R-factors (R_{wp}) were all lower than 3.4%.

The main peak at around 18° in XRD results in Fig. 8 clearly shows that CH is the major crystal product across the S2 and S3 in both temperatures of 20 °C and 40 °C. On the other hand, the amount of ettringite is almost negligible since there are no peaks at 9–9.5° in the XRD results. Thereby, the general XRD results confirm that CH is the main crystal phase that induces crystallization pressure on the pore walls and then causes autogenous expansion. By comparing the CH content (calculated by the Rietveld refinement) at different ages with the AD, as shown in Fig. 9, patterns regarding the mechanisms of AD in S2~S4 and the influence of temperature can be described as follows: 1) In S2, the fast increase of CH corresponds to the fast autogenous expansion. The CH production rates in S2 for 20 °C and 40 °C are 0.18% wt./hour and 0.82% wt./hour respectively; 2) After S2, the CH production rates for 20 °C and 40 °C are 0.06% wt./hour and 0.03% wt./hour respectively. In other words, after S2, the CH production rate in 20 °C decreases to 33.33% of the previous stage, while in 40 °C, the CH production rate accounts only for 3.65% of the previous stage. The patterns described above explain the mechanisms of autogenous expansion in S2 and the plateau in S3. In S2, the fast increase of CH induces the autogenous expansion in both temperatures. After S2, in lower temperature, the CH production rate decreases gradually, but the continuous production of CH is still able to apply the crystallization pressure (that induces expansion) to counteract the capillary pressure caused by self-desiccation (that induces shrinkage) [19], and therefore causes the plateau of AD and EAS in S3. On the other hand, in higher temperature, the CH production rate drastically decreases after S2 and the produced CH does not provide enough crystallization pressure that can balance the capillary pressure caused by self-desiccation. As a result, in higher temperature, self-desiccation effects take over much sooner and there is no plateau at the transition of autogenous expansion and shrinkage.

3.4. Autogenous shrinkage in S4 due to self-desiccation

In S4, rapid autogenous shrinkage and EAS evolution happen, which indicates significant risks of EAC. The mechanism of the autogenous shrinkage in S4 is self-desiccation [69]. The rates of autogenous shrinkage and EAS in S4 at different temperatures are the main factors concerning the EAC risk and have been calculated and shown in Fig. 10. The results indicate that increasing temperature generally causes faster development of autogenous shrinkage and EAS, as also observed by [30,32,65]. However, for temperatures in 10–30 °C, the rates of EAS and autogenous shrinkage are similar, which means that even in low-temperature environment, autogenous shrinkage-induced EAC risk cannot be neglected. At 40 °C, a drastic increase of autogenous shrinkage and EAS rate is observed, which indicates very high EAC risk.

The influence of temperature on the autogenous shrinkage is a complex result of several counteracting factors and is often unsystematic [29]. Specifically, increasing temperature results in the following changes: 1) faster hydration [24,70] and therefore faster drop of RH [15,25]; 2) higher ultimate RH due to the free water equilibrium inside the capillary pores [25,71,72]; 3) a more heterogenous microstructure with coarser porosity and increased mean pore radii [73–76]. According to the Kelvin equation, faster drop of RH increases capillary pressure and therefore causes faster autogenous shrinkage, while coarser porosity reduces the capillary pressure and therefore results in slower autogenous shrinkage rate [19]. In general, it seems that the faster hydration and decrease of RH is the main mechanism of the influence of temperature on autogenous shrinkage in the studied ages, since the overall trend of the test shows a positive correlation between temperature and autogenous shrinkage rate. However, it should be noted that such influence is not significant in 10–30 °C, as also observed by many other studies [29,56,65] that the rate of autogenous shrinkage under different temperatures (in the range of 10–30 °C) remains similar. Therefore, a comparable trade-off between the aforementioned three factors may be achieved in the temperature range of 10–30 °C, and results in a similar rate of autogenous shrinkage. When the temperature increases to 40 °C, a significant increase of the AD rate (and therefore the EAS rate) is observed, indicating that the fast hydration and RH drop is the governing mechanism among the aforementioned three factors. Such drastic increase of autogenous shrinkage at 40 °C was also observed by [63,66,77].

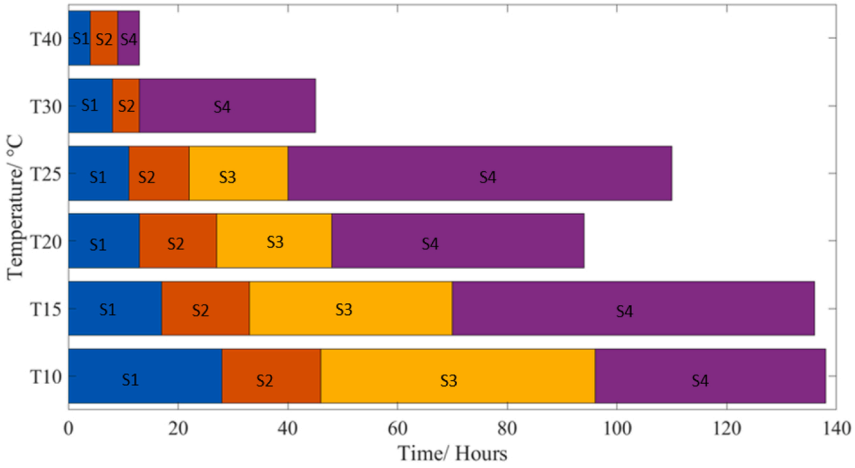

Fig. 8. Durations of the four stages of AD and EAS evolution under different temperatures.

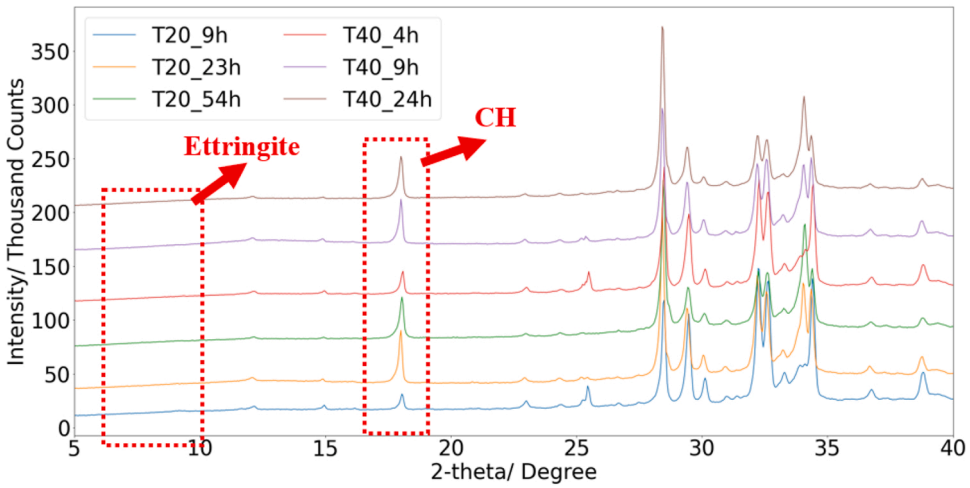

Fig. 9. XRD and Rietveld refinement of the six selected samples at different ages.

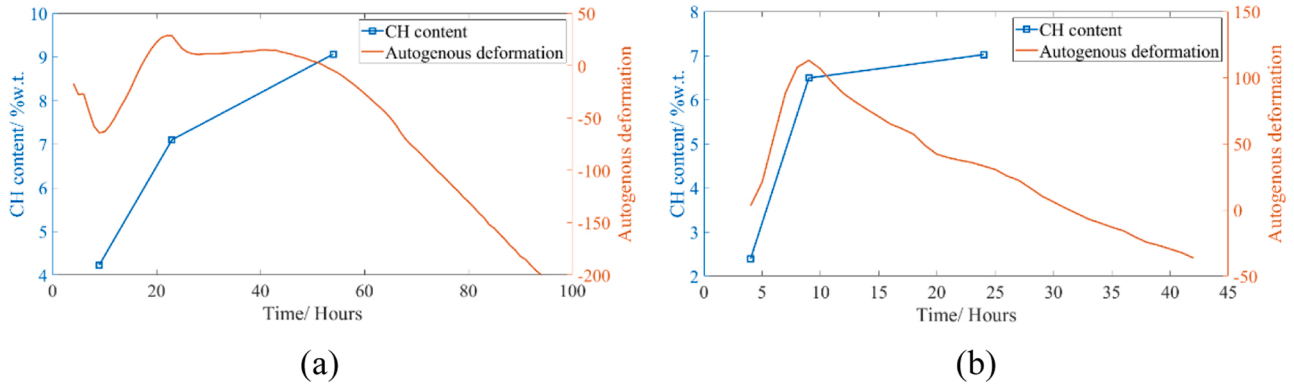

Fig. 10. CH content and the AD of the selected samples: (a) 20 °C; (b) 40 °C.

3.5. Predicting the EAS under different temperatures based on MC

The prediction of EAS under different temperatures is conducted based on the viscoelastic model in the Section 2.5. The required inputs are AD and relaxation modulus, as tested in [40]. Based on the Section 3.1, the MC is not applicable to AD. Thereby, the tested ADs under different temperatures are directly used as input for the model. On the other hand, the relaxation modulus is obtained based on the conversion method of Eq. (9), which uses the elastic modulus and creep compliance function as input. As a property that is positively correlated to the compressive strength, as revealed by macroscale loading-unloading tests [78], the evolution of elastic modules under different temperatures can be successfully predicted by the MC [70,79]. The influence of temperature on creep was mainly influenced by two different mechanisms [80]: 1) Temperature increase accelerates the bond breakages and restorations causing creep, and thus increases the creep rate [81,82]; 2) A temperature increase accelerates the hydration and therefore reduces the creep. For early-age concrete, the effect of hydration dominates and therefore the MC can still be used for predicting the basic creep at the early age [80,83]. The increase of RH can increase the long-term creep rate [82,84], and can be quantified by the microprestress-solidification theory [80,85].

Therefore, in this section, the MC is applied to first calculate the elastic modulus and creep compliance at different temperatures based on the testing results under 20 °C [40]. Then, the relaxation modulus at different temperatures can be further calculated by MC and the Eq.(9) using the elastic modulus and creep compliance as the input. Part of the relaxation modulus at four different times of loading (i.e., 12, 24, 48, 72 h) at different temperatures are shown in Fig. 11. The results show that as the time of loading and temperature increase, the relaxation modulus increases, which is reasonable because a later timing of loading indicates longer hydration and higher temperatures accelerate the hydration. Using the calculated relaxation modulus and the tested AD as the input for Eq. (7), the EAS at different temperatures can be predicted, as shown in Fig. 12. Root Mean Square Error (RMSE) is calculated (see Eq.(10)) to show the difference between the predicted and tested EAS. The results show that, using the relaxation modulus converted by the MC as the input, the viscoelastic model can still predict the EAS at different temperatures with only limited errors in some cases. Such error may be attributed to the variation in the different batches of the cement. The prediction of the EAS under different temperatures shows that the MC is applicable to the early-age viscoelastic properties (i.e., elastic modulus and creep/ relaxation).

4. Conclusions

Based on the Mini-TSTM/ ADTM tests under different temperatures, this paper revealed the influence of temperature on the four-stage process of the AD and EAS in restrained cementitious materials. XRD tests were performed to investigate in-depth the micro-scale mechanisms of autogenous expansion. The applicability of MC on the prediction of AD and relaxation modulus was also examined by experimental data and the viscoelastic model. The following can therefore be concluded in this paper:

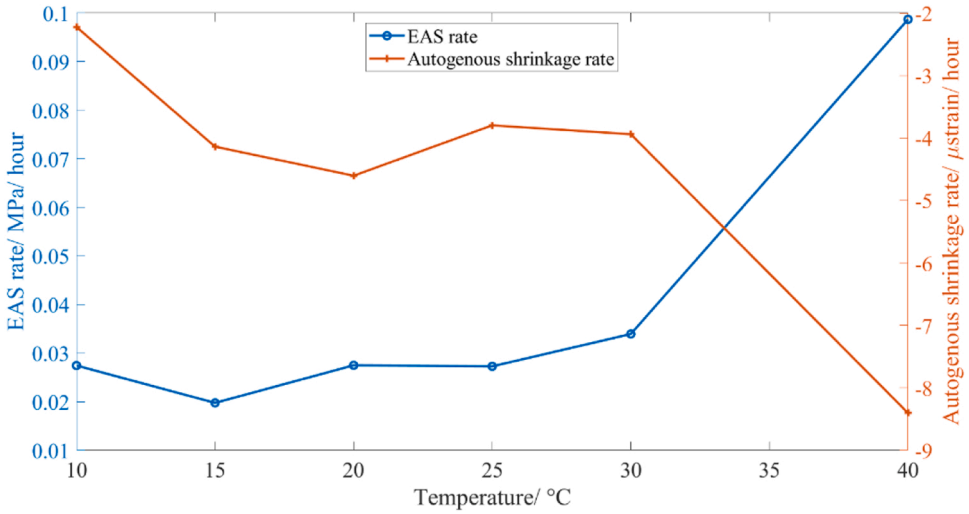

Fig. 11. Rate of EAS and AD in S4.

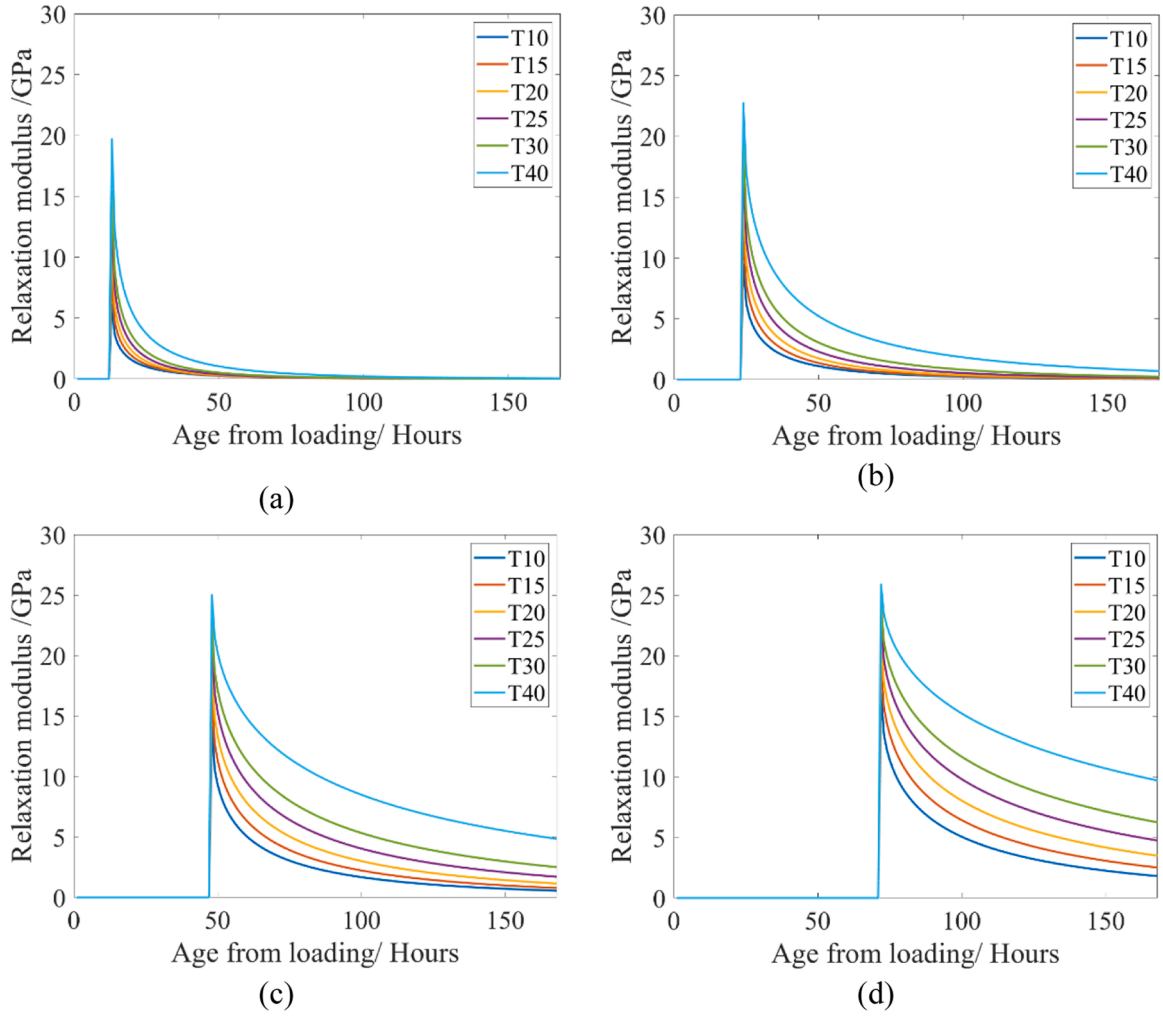

Fig. 12. Relaxation modulus at different temperatures (a-d) are for time of loading (t_0) since 12, 24, 48, and 72 h respectively.

1) The AD of ordinary Portland cement paste can be described as a four-stage process: the initial deformation (i.e., time-zero), autogenous expansion, plateau, and autogenous shrinkage. Due to the low elastic modulus and high creep in the first two stages, the magnitude of EAS is low. The plateau in the third stage delays the occurrence of tensile stress which will accumulate drastically in the fourth stage when autogenous shrinkage is induced by self-desiccation.
2) Higher temperatures can increase the risk of EAC. Higher temperatures accelerate the transition through the initial stages, causing the autogenous shrinkage stage to occur earlier. Beyond 30 °C, the

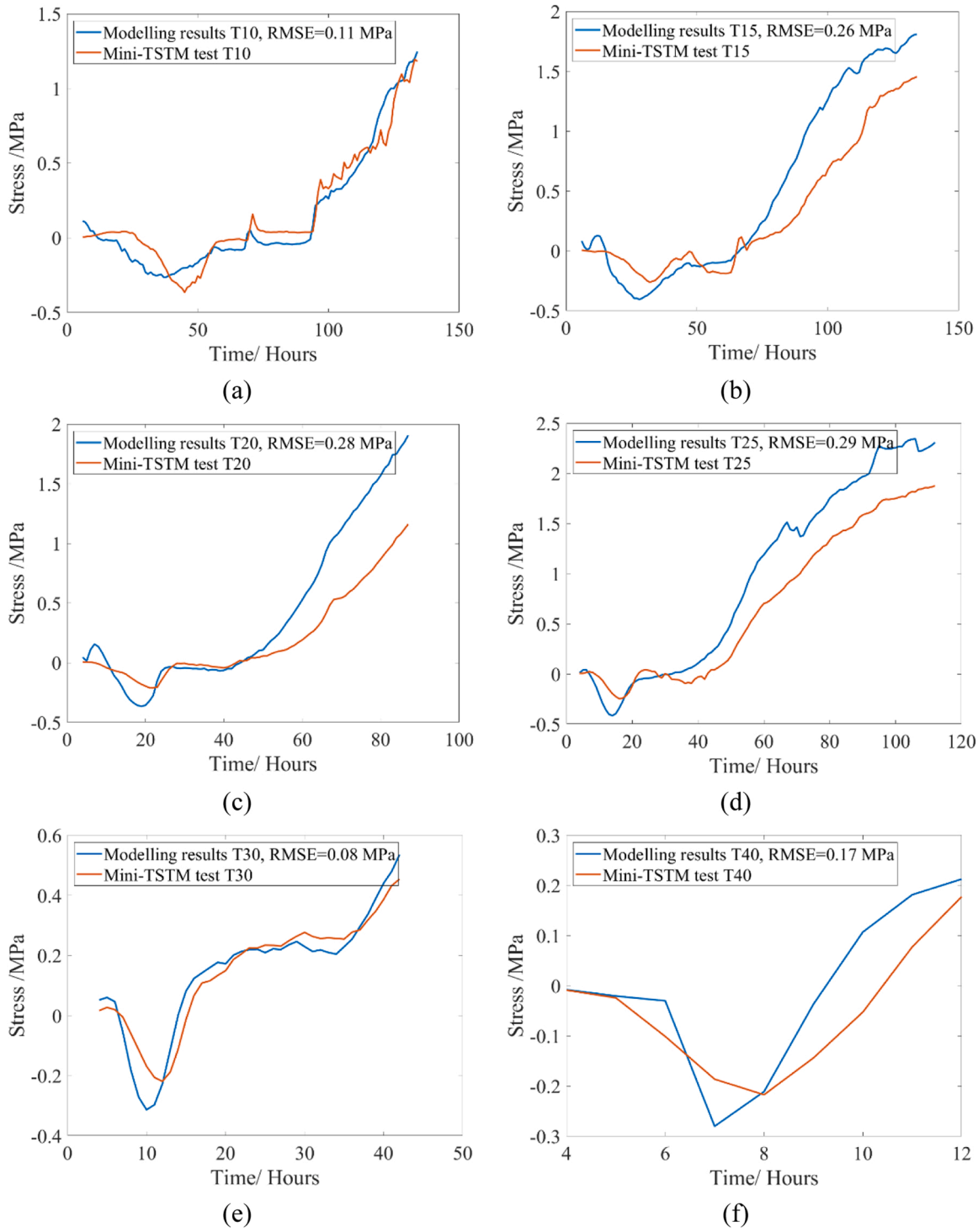

Fig. 13. Predicted EAS evolution at different temperatures (a-f) are for different temperatures of 10 °C, 15 °C, 20 °C, 25 °C, 30 °C, and 40 °C respectively.

plateau stage disappears, directly linking autogenous expansion to autogenous shrinkage. Moreover, higher temperatures lead to increased rates of autogenous shrinkage and EAS.

3) The autogenous expansion and plateau of slow deformation are attributed to the CH content, as quantified by the XRD analysis. At the beginning of the second stage, the fast CH production induces the autogenous expansion. As the temperature increases, the CH production rate decreases. At temperatures below 30 °C, the produced CH after the second stage can still apply crystallization pressure to balance the self-desiccation capillary pressure and result in the plateau of slow AD. However, when temperature is above 30 °C, the CH production rate decreases drastically and the self-desiccation effect dominates, resulting in a direct autogenous shrinkage after the second stage. Note that for massive concrete structures where temperature often increases to values above 40 °C, the plateau of slow AD disappears and a direct autogenous shrinkage happens after the second stage, increasing the EAC risk.
4) Low-temperature curing delays but does not entirely prevent AD-induced EAC. In moderate temperatures (10–30 °C), the rates of

autogenous shrinkage and EAS in the fourth stage are approximately at the same level, leading to the EAC issues at the end.

5) While the MC does not accurately predict AD across temperatures, it successfully calculates relaxation modulus. This, in turn, aids in EAS estimation based on AD data.

CRediT authorship contribution statement

Šavija Branko: Writing – review & editing, Supervision, Investigation, Funding acquisition. **Chang Ze:** Writing – review & editing, Investigation. **Schlangen Erik:** Writing – original draft, Supervision, Investigation, Funding acquisition. **Liu Chen:** Writing – review & editing, Methodology, Investigation, Formal analysis. **Liang Xuhui:** Writing – review & editing, Investigation. **Liang Minfei:** Writing – review & editing, Writing – original draft, Methodology, Investigation, Formal analysis, Data curation, Conceptualization.

Declaration of Competing Interest

The authors declare that they have no known competing financial interests or personal relationships that could have appeared to influence the work reported in this paper.

Data Availability

Data will be made available on request.

Acknowledgements

Minfei Liang and Chen Liu would like to acknowledge the funding supported by China Scholarship Council under grant number 202007000027 and 201906950102, respectively. Branko Šavija acknowledges the financial support of the European Research Council (ERC) within the framework of the ERC Starting Grant Project “Auxetic Cementitious Composites by 3D printing (ACC-3D)”, Grant Agreement Number 101041342.

References

[1] I. Maruyama, P. Lura, Properties of early-age concrete relevant to cracking in massive concrete, Cem. Concr. Res. 123 (2019), 105770, https://doi.org/10.1016/J.CEMCONRES.2019.05.015.

[2] Md Safiuddin, A. Kaish, C.-O. Woon, S. Raman, Early-age cracking in concrete: causes, consequences, remedial measures, and recommendations, Appl. Sci. 8 (2018) 1730, https://doi.org/10.3390/app8101730.

[3] D. Huang, P. Chen, H. Peng, Y. Yang, Q. Yuan, M. Su, A review and comparison study on drying shrinkage prediction between alkali-activated fly ash/slag and ordinary Portland cement, Constr. Build. Mater. 305 (2021), 124760, https://doi.org/10.1016/j.conbuildmat.2021.124760.

[4] B. Klemczak, A. Żmij, Reliability of standard methods for evaluating the early-age cracking risk of thermal-shrinkage origin in concrete walls, Constr. Build. Mater. 226 (2019) 651–661, https://doi.org/10.1016/j.conbuildmat.2019.07.167.

[5] J. Xin, Y. Liu, G. Zhang, Z. Wang, J. Wang, N. Yang, Y. Qiao, Evaluation of early-age thermal cracking resistance of high w/b, high volume fly ash (HVFA) concrete using temperature stress testing machine, Case Stud. Constr. Mater. 16 (2022), e00825, https://doi.org/10.1016/j.cscm.2021.e00825.

[6] J. Yang, Q. Wang, Y. Zhou, Influence of curing time on the drying shrinkage of concretes with different binders and water-to-binder ratios, Adv. Mater. Sci. Eng. 2017 (2017) 1–10, https://doi.org/10.1155/2017/2695435.

[7] Z. Hu, C. Shi, Z. Cao, Z. Ou, D. Wang, Z. Wu, L. He, A review on testing methods for autogenous shrinkage measurement of cement-based materials, J. Sustain. Cem. Based Mater. 2 (2013) 161–171, https://doi.org/10.1080/21650373.2013.797937.

[8] L. Wu, N. Farzadnia, C. Shi, Z. Zhang, H. Wang, Autogenous shrinkage of high performance concrete: a review, Constr. Build. Mater. 149 (2017) 62–75, https://doi.org/10.1016/j.conbuildmat.2017.05.064.

[9] L. Yang, C. Shi, Z. Wu, Mitigation techniques for autogenous shrinkage of ultra-high-performance concrete – A review, Compos B Eng. 178 (2019), 107456, https://doi.org/10.1016/J.COMPOSITESB.2019.107456.

[10] X. Zhang, Z. Liu, F. Wang, Autogenous shrinkage behavior of ultra-high performance concrete, Constr. Build. Mater. 226 (2019) 459–468, https://doi.org/10.1016/j.conbuildmat.2019.07.177.

[11] A. Markandeya, D.G. Mapa, M. Fincan, N. Shanahan, Y.P. Stetsko, K.A. Riding, A. Zayed, Chemical shrinkage and cracking resilience of metakaolin concrete, Acids Mater. J. 116 (2019) 99–106, https://doi.org/10.14359/51716714.

[12] K. Orosz, H. Hedlund, A. Cwirzen, Effects of variable curing temperatures on autogenous deformation of blended cement concretes, Constr. Build. Mater. 149 (2017) 474–480, https://doi.org/10.1016/j.conbuildmat.2017.05.143.

[13] P. Lura, O.M. Jensen, K. Van Breugel, Autogenous shrinkage in high-performance cement paste: an evaluation of basic mechanisms, Cem. Concr. Res 33 (2003) 223–232, https://doi.org/10.1016/S0008-8846(02)00890-6.

[14] L. Barcelo, M. Moranville, B. Clavaud, Autogenous shrinkage of concrete: a balance between autogenous swelling and self-desiccation, Cem. Concr. Res 35 (2005) 177–183, https://doi.org/10.1016/j.cemconres.2004.05.050.

[15] J. Carette, S. Staquet, Unified modelling of the temperature effect on the autogenous deformations of cement-based materials, Cem. Concr. Compos 94 (2018) 62–71, https://doi.org/10.1016/j.cemconcomp.2018.08.008.

[16] J. Carette, S. Joseph, Ö. Cizer, S. Staquet, Decoupling the autogenous swelling from the self-desiccation deformation in early age concrete with mineral additions: micro-macro observations and unified modelling, Cem. Concr. Compos 85 (2018) 122–132, https://doi.org/10.1016/j.cemconcomp.2017.10.008.

[17] M. Liang, Z. Chang, Y. Zhang, H. Cheng, S. He, E. Schlangen, B. Šavija, Autogenous deformation induced- stress evolution in high-volume GGBFS concrete: Macro-scale behavior and micro-scale origin, Constr. Build. Mater. 370 (2023), 130663, https://doi.org/10.1016/j.conbuildmat.2023.130663.

[18] M. Liang, Z. Li, S. He, Z. Chang, Y. Gan, E. Schlangen, B. Šavija, Stress evolution in restrained GGBFS concrete due to autogenous deformation: bayesian optimization of aging creep, Constr. Build. Mater. 324 (2022), 126690, https://doi.org/10.1016/J.CONBUILDMAT.2022.126690.

[19] S. Tang, D. Huang, Z. He, A review of autogenous shrinkage models of concrete, J. Build. Eng. 44 (2021), 103412, https://doi.org/10.1016/j.jobe.2021.103412.

[20] M.N. Amin, J.-S. Kim, T.T. Dat, J.-K. Kim, Improving test methods to measure early age autogenous shrinkage in concrete based on air cooling, IES J. Part A: Civ. Struct. Eng. 3 (2010) 244–256, https://doi.org/10.1080/19373260.2010.522314.

[21] S. Staquet, B. Delsaute, A. Darquennes, B. Espion, Design of a revisited TSTM system for testing concrete since setting time under free and restraint conditions, in: CONCRACK 3 – RILEM-JCI International Workshop on Crack Control of Mass Concrete and Related Issues Concerning Early-Age of Concrete Structures, Paris, France, 2012.

[22] M.H. Zhang, C.T. Tam, M.P. Leow, Effect of water-to-cementitious materials ratio and silica fume on the autogenous shrinkage of concrete, Cem. Concr. Res 33 (2003) 1687–1694, https://doi.org/10.1016/S0008-8846(03)00149-2.

[23] A.E. Klausen, T. Kanstad, Ø. Bjøntegaard, E.J. Sellevold, The effect of curing temperature on autogenous deformation of fly ash concretes, Cem. Concr. Compos 109 (2020), 103574, https://doi.org/10.1016/j.cemconcomp.2020.103574.

[24] P. F. Hansen, J. Pedersen, Maturity computer for controlled curing and hardening of concrete, Nord. Beton 1 (1977) 19–34.

[25] O.M. Jensen, P.F. Hansen, Influence of temperature on autogenous deformation and relative humidity change in hardening cement paste, Cem. Concr. Res 29 (1999) 567–575, https://doi.org/10.1016/S0008-8846(99)00021-6.

[26] Ø. Bjøntegaard, E.J. Sellevold, Interaction between thermal dilation and autogenous deformation in high performance concrete, Mater. Struct. 34 (2001) 266–272, https://doi.org/10.1007/BF02482205.

[27] C. Jiang, Y. Yang, Y. Wang, Y. Zhou, C. Ma, Autogenous shrinkage of high performance concrete containing mineral admixtures under different curing temperatures, Constr. Build. Mater. 61 (2014) 260–269, https://doi.org/10.1016/J.CONBUILDMAT.2014.03.023.

[28] H.-W. Reinhardt, M. Stegmaier, Influence of heat curing on the pore structure and compressive strength of self-compacting concrete (SCC), Cem. Concr. Res 36 (2006) 879–885, https://doi.org/10.1016/j.cemconres.2005.12.004.

[29] P. Lura, K. van Breugel, I. Maruyama, Effect of curing temperature and type of cement on early-age shrinkage of high-performance concrete, Cem. Concr. Res 31 (2001) 1867–1872, https://doi.org/10.1016/S0008-8846(01)00601-9.

[30] A. Loukili, D. Chopin, A. Khelidj, J.-Y. Le Touzo, A new approach to determine autogenous shrinkage of mortar at an early age considering temperature history, Cem. Concr. Res 30 (2000) 915–922, https://doi.org/10.1016/S0008-8846(00)00241-6.

[31] I. Chu, S.H. Kwon, M.N. Amin, J.-K. Kim, Estimation of temperature effects on autogenous shrinkage of concrete by a new prediction model, Constr. Build. Mater. 35 (2012) 171–182, https://doi.org/10.1016/j.conbuildmat.2012.03.005.

[32] D. Shen, J. Jiang, J. Shen, P. Yao, G. Jiang, Influence of curing temperature on autogenous shrinkage and cracking resistance of high-performance concrete at an early age, Constr. Build. Mater. 103 (2016) 67–76, https://doi.org/10.1016/J.CONBUILDMAT.2015.11.039.

[33] L. Li, V. Dao, P. Lura, Autogenous deformation and coefficient of thermal expansion of early-age concrete: Initial outcomes of a study using a newly-developed Temperature Stress Testing Machine, Cem. Concr. Compos 119 (2021), 103997, https://doi.org/10.1016/j.cemconcomp.2021.103997.

[34] I. Maruyama, A. Teramoto, Temperature dependence of autogenous shrinkage of silica fume cement pastes with a very low water–binder ratio, Cem. Concr. Res 50 (2013) 41–50, https://doi.org/10.1016/j.cemconres.2013.03.017.

[35] H. Zhu, Y. Hu, R. Ma, J. Wang, Q. Li, Concrete thermal failure criteria, test method, and mechanism: A review, Constr. Build. Mater. 283 (2021), 122762, https://doi.org/10.1016/j.conbuildmat.2021.122762.

[36] A. Bentur, K. Kovler, Evaluation of early age cracking characteristics in cementitious systems, Mater. Struct. 36 (2003) 183–190, https://doi.org/10.1007/BF02479556.

[37] J. Xin, G. Zhang, Y. Liu, Z. Wang, Z. Wu, Evaluation of behavior and cracking potential of early-age cementitious systems using uniaxial restraint tests: A review, Constr. Build. Mater. 231 (2020), 117146, https://doi.org/10.1016/J.CONBUILDMAT.2019.117146.
[38] S. Staquet, B. Delsaute, A. Darquennes, B. Espion, DESIGN OF A REVISITED TSTM SYSTEM FOR TESTING CONCRETE SINCE SETTING TIME UNDER FREE AND RESTRAINT CONDITIONS, 2012.
[39] D.H. Nguyen, V.T. Nguyen, P. Lura, V.T.N. Dao, Temperature-stress testing machine – A state-of-the-art design and its unique applications in concrete research, Cem. Concr. Compos 102 (2019) 28–38, https://doi.org/10.1016/J.CEMCONCOMP.2019.04.019.
[40] M. Liang, Z. Chang, P. Holthuizen, Y. Chen, S. He, E. Schlangen, B. Šavija, Efficiently Assessing the Early-Age Cracking Risk of Cementitious Materials with A Mini Temperature Stress Testing Machine, (2023).
[41] M. Irfan-ul-Hassan, B. Pichler, R. Reihsner, Ch Hellmich, Elastic and creep properties of young cement paste, as determined from hourly repeated minute-long quasi-static tests, Cem. Concr. Res 82 (2016) 36–49, https://doi.org/10.1016/j.cemconres.2015.11.007.
[42] C. Boulay, S. Staquet, B. Delsaute, J. Carette, M. Crespini, O. Yazoghli-Marzouk, É. Merliot, S. Ramanich, How to monitor the modulus of elasticity of concrete, automatically since the earliest age? Mater. Struct. /Mater. Et. Constr. 47 (2014) 141–155, https://doi.org/10.1617/s11527-013-0051-3.
[43] K. van Breugel, Simulation of hydration and Formation of Structure in Hardening Cement-Based, Mater., TU Delft (1991).
[44] Methods for Calculating Activation Energy for Portland Cement, ACI Mater. J. 104 (2007), https://doi.org/10.14359/18499.
[45] J.R. van Bokhorst, Early-age cracking of concrete A study into the influence of stress relaxation on early-age cracking of concrete structures under imposed deformations, n.d. http://repository.tudelft.nl/.
[46] Y. Gao, J. Zhang, P. Han, Determination of stress relaxation parameters of concrete in tension at early-age by ring test, Constr. Build. Mater. 41 (2013) 152–164, https://doi.org/10.1016/j.conbuildmat.2012.12.004.
[47] M. Azenha, F. Kanavaris, D. Schlicke, A. Jędrzejewska, F. Benboudjema, T. Honorio, V. Šmilauer, C. Serra, J. Forth, K. Riding, B. Khadka, C. Sousa, M. Briffaut, L. Lacarrière, E. Koenders, T. Kanstad, A. Klausen, J.M. Torrenti, E.M. R. Fairbairn, Recommendations of RILEM TC 287-CCS: thermo-chemo-mechanical modelling of massive concrete structures towards cracking risk assessment, Mater. Struct. /Mater. Et. Constr. 54 (2021), 135, https://doi.org/10.1617/s11527-021-01732-8.
[48] Z.P. Bažant, M. Jirásek, Creep and Hygrothermal Effects in Concrete Structures, Springer Netherlands,, Dordrecht, 2018, https://doi.org/10.1007/978-94-024-1138-6.
[49] Z.P. Bazant, E. Osman, Double power law for basic creep of concrete, Matér. Et. Constr. 9 (1976) 3–11.
[50] F. Wittmann, Bestimmung physikalischer Eigenschaften des Zementsteins, 1974.
[51] K. Van Breugel, Relaxation of Young Concrete, 1980.
[52] Z. Li, S. Zhang, X. Liang, G. Ye, Cracking potential of alkali-activated slag and fly ash concrete subjected to restrained autogenous shrinkage, Cem. Concr. Compos 114 (2020), https://doi.org/10.1016/j.cemconcomp.2020.103767.
[53] D.-Y. Yoo, N. Banthia, Y.-S. Yoon, Effectiveness of shrinkage-reducing admixture in reducing autogenous shrinkage stress of ultra-high-performance fiber-reinforced concrete, Cem. Concr. Compos 64 (2015) 27–36, https://doi.org/10.1016/j.cemconcomp.2015.09.005.
[54] M. Liang, Z. Chang, S. He, Y. Chen, Y. Gan, E. Schlangen, B. Šavija, Predicting early-age stress evolution in restrained concrete by thermo-chemo-mechanical model and active ensemble learning, Comput. -Aided Civ. Infrastruct. Eng. 37 (2022) 1809–1833, https://doi.org/10.1111/mice.12915.
[55] M. Wyrzykowski, Z. Hu, S. Ghourchian, K. Scrivener, P. Lura, Corrugated tube protocol for autogenous shrinkage measurements: review and statistical assessment, Mater. Struct. 50 (2017), 57, https://doi.org/10.1617/s11527-016-0933-2.
[56] Pietro Lura, Autogenous Deformation and Internal Curing of Concrete, Delft University of Technology,, 2003.
[57] A.E. Klausen, Early age crack assessment of concrete structures, experimental determination of decisive parameters, Ph.D. thesis, NTNU, 2016.
[58] A. Darquennes, S. Staquet, B. Espion, Determination of time-zero and its effect on autogenous deformation evolution, Eur. J. Environ. Civ. Eng. 15 (2011) 1017–1029, https://doi.org/10.1080/19648189.2011.9695290.
[59] J.R.T. Filho, M.A.P.G. de Araújo, D. Snoeck, N. De Belie, Discussing different approaches for the time-zero as start for autogenous shrinkage in cement pastes containing superabsorbent polymers, Materials 12 (2019), https://doi.org/10.3390/ma12182962.
[60] H. Huang, G. Ye, Examining the "time-zero" of autogenous shrinkage in high/ultra-high performance cement pastes, Cem. Concr. Res 97 (2017) 107–114, https://doi.org/10.1016/J.CEMCONRES.2017.03.010.
[61] A. Bentur, M. Ish-Shalom, Properties of type K expensive cement of pure components II. Proposed mechanism of ettringite formation and expansion in unrestrained paste of pure expansive component, Cem. Concr. Res 4 (1974) 709–721, https://doi.org/10.1016/0008-8846(74)90043-X.
[62] P.K. Mehta, Mechanism of expansion associated with ettringite formation, Cem. Concr. Res 3 (1973) 1–6, https://doi.org/10.1016/0008-8846(73)90056-2.
[63] V. Baroghel-Bouny, P. Mounanga, A. Khelidj, A. Loukili, N. Rafaï, Autogenous deformations of cement pastes, Cem. Concr. Res 36 (2006) 123–136, https://doi.org/10.1016/j.cemconres.2004.10.020.
[64] P. Lura, O.M. Jensen, J. Weiss, Cracking in cement paste induced by autogenous shrinkage, Mater. Struct. /Mater. Et. Constr. 42 (2009) 1089–1099, https://doi.org/10.1617/s11527-008-9445-z.
[65] C. Jiang, Y. Yang, Y. Wang, Y. Zhou, C. Ma, Autogenous shrinkage of high performance concrete containing mineral admixtures under different curing temperatures, Constr. Build. Mater. 61 (2014) 260–269, https://doi.org/10.1016/j.conbuildmat.2014.03.023.
[66] P. Mounanga, V. Baroghel-Bouny, A. Loukili, A. Khelidj, Autogenous deformations of cement pastes: Part I. Temperature effects at early age and micro–macro correlations, Cem. Concr. Res 36 (2006) 110–122, https://doi.org/10.1016/j.cemconres.2004.10.019.
[67] H.M. Rietveld, A Profile Refinement Method for Nuclear and Magnetic Structures, J. Appl. Crystallogr 2 (1969) 65–71.
[68] N. Doebelin, R. Kleeberg, Profex: A graphical user interface for the Rietveld refinement program BGMN, J. Appl. Crystallogr 48 (2015), https://doi.org/10.1107/S1600576715014685.
[69] T. Lu, Z. Li, K. van Breugel, Modelling of autogenous shrinkage of hardening cement paste, Constr. Build. Mater. 264 (2020), https://doi.org/10.1016/j.conbuildmat.2020.120708.
[70] V. Waller, L. d'Aloïa, F. Cussigh, S. Lecrux, Using the maturity method in concrete cracking control at early ages, Cem. Concr. Compos 26 (2004) 589–599, https://doi.org/10.1016/S0958-9465(03)00080-5.
[71] S. Poyet, Experimental investigation of the effect of temperature on the first desorption isotherm of concrete, Cem. Concr. Res 39 (2009) 1052–1059, https://doi.org/10.1016/j.cemconres.2009.06.019.
[72] J.M. de Burgh, S.J. Foster, Influence of temperature on water vapour sorption isotherms and kinetics of hardened cement paste and concrete, Cem. Concr. Res 92 (2017) 37–55, https://doi.org/10.1016/j.cemconres.2016.11.006.
[73] A.A. Almusallam, Effect of environmental conditions on the properties of fresh and hardened concrete, Cem. Concr. Compos 23 (2001) 353–361, https://doi.org/10.1016/S0958-9465(01)00007-5.
[74] J.I. Escalante-García, J.H. Sharp, Effect of temperature on the hydration of the main clinker phases in portland cements: part i, neat cements, Cem. Concr. Res 28 (1998) 1245–1257, https://doi.org/10.1016/S0008-8846(98)00115-X.
[75] B. Lothenbach, F. Winnefeld, C. Alder, E. Wieland, P. Lunk, Effect of temperature on the pore solution, microstructure and hydration products of Portland cement pastes, Cem. Concr. Res 37 (2007) 483–491, https://doi.org/10.1016/j.cemconres.2006.11.016.
[76] K.O. Kjellsen, R.J. Detwiler, O.E. Gjørv, Development of microstructures in plain cement pastes hydrated at different temperatures, Cem. Concr. Res 21 (1991) 179–189, https://doi.org/10.1016/0008-8846(91)90044-I.
[77] P. Turcry, A. Loukili, L. Barcelo, J.M. Casabonne, Can the maturity concept be used to separate the autogenous shrinkage and thermal deformation of a cement paste at early age? Cem. Concr. Res 32 (2002) 1443–1450, https://doi.org/10.1016/S0008-8846(02)00800-1.
[78] M.A. Rashid, M.A. Mansur, P. Paramasivam, Correlations between Mechanical Properties of High-Strength Concrete, J. Mater. Civ. Eng. 14 (2002) 230–238, https://doi.org/10.1061/(ASCE)0899-1561(2002)14:3(230).
[79] D. Geng, N. Dai, X. Jin, E. Miao, Comparison of calculating methods and applications of different concrete maturity, J. Phys. Conf. Ser. 2011 (2021), 012022, https://doi.org/10.1088/1742-6596/2011/1/012022.
[80] Z.P. Bažant, G. Cusatis, L. Cedolin, Temperature Effect on Concrete Creep Modeled by Microprestress-Solidification Theory, J. Eng. Mech. 130 (2004) 691–699, https://doi.org/10.1061/(ASCE)0733-9399(2004)130:6(691).
[81] M. Briffaut, F. Benboudjema, J.M. Torrenti, G. Nahas, Concrete early age basic creep: Experiments and test of rheological modelling approaches, Constr. Build. Mater. 36 (2012) 373–380, https://doi.org/10.1016/j.conbuildmat.2012.04.101.
[82] M. Liang, Z. Chang, Z. Wan, Y. Gan, E. Schlangen, B. Šavija, Interpretable Ensemble-Machine-Learning models for predicting creep behavior of concrete, Cem. Concr. Compos 125 (2022), 104295, https://doi.org/10.1016/J.CEMCONCOMP.2021.104295.
[83] G. De Schutter, Applicability of degree of hydration concept and maturity method for thermo-visco-elastic behaviour of early age concrete, Cem. Concr. Compos 26 (2004) 437–443, https://doi.org/10.1016/S0958-9465(03)00067-2.
[84] J. Frech-Baronet, L. Sorelli, J.P. Charron, New evidences on the effect of the internal relative humidity on the creep and relaxation behaviour of a cement paste by micro-indentation techniques, Cem. Concr. Res 91 (2017) 39–51, https://doi.org/10.1016/J.CEMCONRES.2016.10.005.
[85] P. Yu, Y.H. Duan, Q.X. Fan, S.W. Tang, Improved MPS model for concrete creep under variable humidity and temperature, Constr. Build. Mater. 243 (2020), 118183, https://doi.org/10.1016/j.conbuildmat.2020.118183.